Title

The effect of Cu additions in FePt–BN–SiO2 heat-assisted magnetic recording media

Journal

Journal of Physics Condensed Matter, 33(10)

ISSN

0953-8984

Authors

Streubel, Robert
N'Diaye, Alpha T
Srinivasan, Kumar
et al.

Publication Date

2021-03-10

DOI

10.1088/1361-648x/abcff8

Peer reviewed

The effect of Cu additions in FePt-BN-SiO_2 heat-assisted magnetic recording media

Robert Streubel,[1,2,3,*] Alpha T. N'Diaye,[4] Kumar Srinivasan,[5]
Alan Kalitsov,[5] Shikha Jain,[5] Antony Ajan,[5] and Peter Fischer[3,6]

[1] *Department of Physics and Astronomy, University of Nebraska-Lincoln, Lincoln, NE 68588, USA*
[2] *Nebraska Center for Materials and Nanoscience, University of Nebraska-Lincoln, Lincoln, NE 68588, USA*
[3] *Materials Sciences Division, Lawrence Berkeley National Laboratory, Berkeley CA 94720, USA*
[4] *Advanced Light Source, Lawrence Berkeley National Laboratory, Berkeley CA 94720, USA*
[5] *Western Digital, 5601 Great Oaks Parkway, San Jose, CA 95119, USA*
[6] *Physics Department, UC Santa Cruz, Santa Cruz CA 95064, USA*

Structural and chemical order impact magnetic properties of solids, which are governed by spin-orbit coupling and exchange interaction. The ordered $L1_0$ phase of FePt is a key material to heat-assisted magnetic recording; to enable high storage density, a solid understanding is needed of structural and chemical disorder at small length scales, as well as associated modifications of the electronic band structure. Here, we investigate the effect of boron and copper additions ($\lesssim$ 6 mol.%Cu) on structural and magnetic properties of $L1_0$ FePt granular media. Two copper-driven mechanisms, although competing, can lead to improvements in both structural and magnetic properties. In particular, the Cu substitution on the Fe-site leads to a degradation of magnetic properties due to the delocalized electron orbitals originating from a larger Cu *d*-orbital occupancy. At the same time, Cu substitution leads to an enhanced crystallographic order and consequently magneto-crystalline anisotropy, which offsets the former effect to a large extent. Our study is based on magnetometry, x-ray absorption spectroscopy, ab-initio calculations and a phenomenological theory of disordered FePt granular media. We do not observe a sizable modification to Fe moments and electronic configuration; Cu reveals two different resonances associated with the presence and absence of Cu–B bonds that vary with total Cu concentration.

Recent growth and anticipated near-term explosion in data production require to enhance digital storage and processing capacities of electronic devices. Hard-disk drives utilizing magnetic recording technology remain the dominant auxiliary data storage owing to superior capacity and price advantages over, e.g., solid-state alternatives. At the same time, magnetic recording technology is seeing a transition from perpendicular magnetic recording to other approaches based on energy-assisted switching. One strong contender is heat-assisted magnetic recording (HAMR) based on FePt granular media [1]. The structurally ordered $L1_0$ phase of FePt has one of the highest known magneto-crystalline anisotropies (7×10^7 ergs/cm^3) [2, 3], which allows for engineering thermally stable granular media with record-breaking grain sizes of 3 to 4 nm. With these dimensions, FePt media are capable of reliably storing several terabytes per square inches of data. On the other hand, a large magnetic anisotropy necessitates laser-assisted heating of the FePt medium above its Curie temperature, and synchronized writing of bits during the re-freezing process. Well-defined, magnetically isolated FePt grains are typically manufactured via sputter deposition alongside other constituents or segregants that preferentially form grain boundary phases. Common constituents are carbon, oxides and nitrides; dopants, such as silver and copper, introduced into the FePt matrix are used to tailor, e.g., structural ordering temperature and Curie temperature [4–6]. Please refer to References [2, 3] for a detailed discussion on the terminology of constituents, segregants, and dopants. In a previous work on the spectroscopic study of FePt-C granular films [7], we identified the reduced demagnetization field (grain size) mediated by carbon as the primary cause for the improved magnetic properties with respect to HAMR applications.

Here, we investigate the effect of copper dopants ($\lesssim$ 6 mol.%Cu) on the structural and magnetic properties of $L1_0$ FePt granular media. Previous studies have reported extensively on the effect of Cu on the chemical ordering of the FePt system [8–13]. However, in those cases, the FePt-Cu films were either single-layer non-granular films (no segregants present) or bilayer films formed on a base of granular FePt containing segregants like carbon. In this work, Cu is added incrementally to a single-layer film of FePt-BN-SiO_2 to isolate the effect of Cu independent of the base layer. We find that the formation of nanogranular media is governed by BN and SiO_2 segregants, virtually independent of the Cu concentration. It is recognized by the community that the stoichiometric BN phase does not immediately form, leading to some incorporation of elemental B in the FePt lattice [14]. This assumption is corroborated by an enhancement of magnetic properties after N_2 treatment, reducing the concentration of interstitial boron and degradation of magnetic properties that prevails even without Cu addition. In such films, coercive/saturation field and perpendicular magnetic anisotropy increase with Cu concentration $\lesssim$ 3 mol.%Cu owing to a promoted tetragonal crystallographic order of $L1_0$ FePt. Samples with larger cop-

* streubel@unl.edu

per concentration suffer from an intrinsic degradation of magnetic properties. The competition between the accelerated chemical ordering and degradation of magnetic properties by Cu is analytically treated by advancing the phenomenological theory of FePt granular media [5] to include copper-driven modifications. Harnessing element and chemical specificity of x-ray absorption spectroscopy (XAS) and x-ray magnetic circular dichroism (XMCD) spectroscopy [15, 16], we quantify both spin and orbital moments of iron along the surface normal, and determine the electronic configuration of Cu. The preferred atomic configurations are obtained from ab-initio calculations, analyzing the density of states of Cu 3*d* electrons, and comparing the Cu absorption spectra featuring two resonances that are assigned to magnetic Cu and non-magnetic Cu–B residing on the Fe sublattice, respectively.

I. STRUCTURAL PROPERTIES AND MAGNETIC HYSTERESIS LOOPS

The FePt films were prepared at Western Digital using an industrial-grade Anelva sputter system. All films had the structure glass/seed-layer (50)/heat-sink layer (100)/MgO (5)/$Fe_{1-x}Cu_xPt$-BN-SiO_2 (3)/carbon-overcoat (4). The corresponding layer thickness, shown in brackets, is given in nanometers. The notation for the magnetic layer refers to the composition of the composite target used for sputter deposition, which is chosen to maintain the (Fe+Cu):Pt ratio at equi-atomic levels (1:1), favoring experimentally corroborated Fe-site Cu substitution in $L1_0$ FePt. Note that an unidentified amount of the boron in the plasma does not get nitrogenated and becomes interstitial in the FePt lattice degrading magnetic properties. Details on the exact composition and stack design are considered proprietary information of Western Digital. However, this information is not relevant to structural and magnetic properties, and drawn conclusions. The 3 nm-thick Fe-Pt-Cu-BN-SiO_2 magnetic layers were grown at 600°C substrate temperature in an Ar atmosphere, with Cu concentrations x of 0%, 1.5 mol.%, 3.0 mol.% and 6.0 mol.%. The latter is based on the nominal proportions of the composite target and not measured on individual samples. The structural properties of the granular films are probed in plan and cross-sectional view using an FEI Tecnai transmission electron microscopy (TEM) in scanning and bright-field mode, respectively [Fig. 1(a)]. The grain morphology is quantified by the distribution of grain size and shape (sphericity) [Fig. 1(b)]. The sphericity is defined as the ratio of the two major axes of individual grains approximated as ellipses. From 0 to 6 mol.%Cu, the grain size shrinks from (30.6±17.6) nm^2 to (25.6±17.4) nm^2, while the sphericity increases from 0.63 ± 0.17 to 0.70 ± 0.18. The experimental uncertainty is given by the standard deviation of the corresponding inhomogeneous distributions. These variations are negligible compared with $L1_0$ FePt-C that show a significant decrease in grain size from (200±160) nm^2 down to (50±20) nm^2 for 40 mol.%C concentrations [7]. These observations corroborate that the formation of nanogranular media is driven by the BN and SiO_2 segregant independent of the Cu concentration.

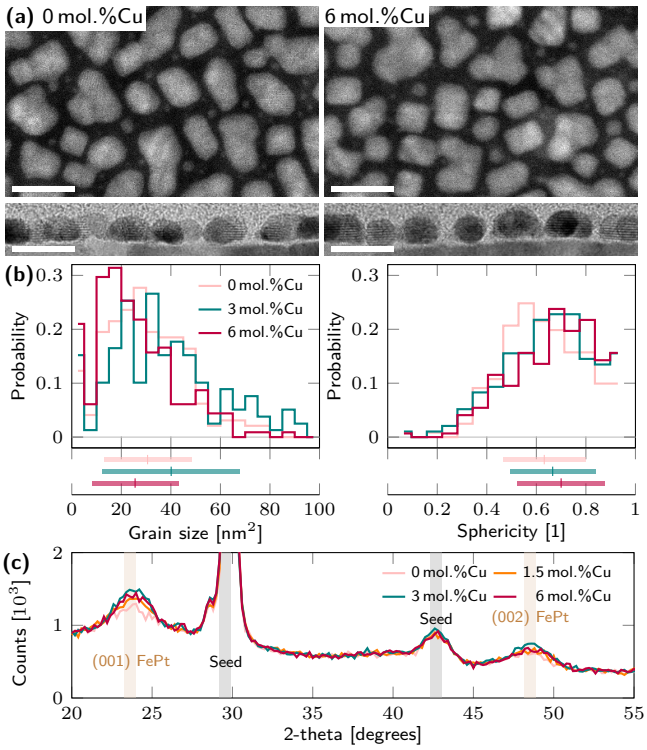

FIG. 1. Structural properties of $L1_0$ Fe-Pt-Cu-B granular media. (a) Top and cross-sectional view of 3 nm-thick FePt films grown at 600°C recorded in STEM-mode and bright-field mode of TEM, respectively. Scale bar is 10 nm. (b) Distribution of grain size and sphericity revealing weak dependence on Cu concentration. (c) Two-theta x-ray diffraction scans confirming crystallographic properties of $L1_0$ FePt.

The key role of copper is to enhance the crystallographic order of $L1_0$ FePt in terms of tetragonality (c-to-a-ratio) and structural order parameter [11, 12]. In the present case, a quantitative analysis of the crystallographic order of 3 nm-thick samples and the influence of Cu is, due to insufficient intensity, challenging with lab-based diffractometry (Philips X'pert diffractometer) [Fig. 1(c)]. This aspect is examined by analyzing the magnetization reversal process in the form of the out-of-plane magnetic hysteresis loops that are governed by the perpendicular magneto-crystalline anisotropy [Fig. 2(a)]. Coercive field, saturation field and remanent magnetization, measured with a 7 T Quantum Design Physical Property Measurement System, increase monotonically with the Cu concentration up to 3 mol.% and reach values 1.5 to 2.5 times of undoped FePt samples [Fig. 2(b)]. The error bars reflect the standard deviation of the determined positive and negative saturation fields owing to a relatively shallow convergence. Contrary to the sat-

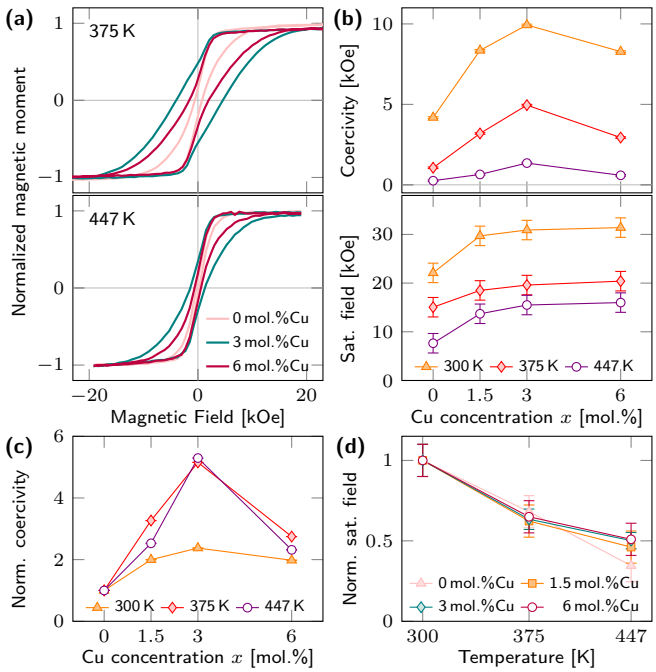

FIG. 2. Magnetic properties derived from vibrating sample magnetometry. (a) Out-of-plane magnetic hysteresis loops measured at different temperatures. (b) Coercive and saturation field unveiling maximum and onset saturation at 3 mol.%Cu, respectively, independent of temperature. (c) Coercive field normalized to FePt with 0 mol.%Cu. (d) Saturation field normalized to room temperature showing distinct temperature dependence for doped and undoped FePt samples.

uration field, which retains its saturation value, both coercive field and remanent magnetization decrease for > 3 mol.%Cu. The relative change of the latter is larger for elevated temperatures closer to the Curie temperature of ≈ 650 K [Fig. 2(c)].

II. X-RAY ABSORPTION SPECTROSCOPY

Further insight into chemical and magnetic properties is given by XAS and XMCD spectroscopy performed at beamline 6.3.1 at the Advanced Light Source (Berkeley, CA). The XAS near the Fe $L_{3,2}$ edges [$(690 \sim 750)$ eV] are recorded in the presence of an external magnetic field (± 18.8 kOe) normal to the sample surface. The spectra are retrieved from the current of electrons emanating from the surface (total electron yield), which provide a probing depth of about 6 nm and hence information about the entire FePt system. Each spectrum is normalized to the intensity of the pre-edge, followed by a subtraction of 1, to compensate for changes in beam intensity. Contributions from inelastically scattered electrons are approximated using the Shirley background and subtracted from each individual spectra [17]. The spectra plotted in Figure 3(a) are typical for metallic FePt [18, 19]. Calculating the integrals of both XAS and XMCD spectra $r = \int_{L_3+L_2} (\mu_+ + \mu_-)\,\mathrm{d}\omega\,, q = \int_{L_3+L_2} (\mu_+ - \mu_-)\,\mathrm{d}\omega\,, p = \int_{L_3} (\mu_+ - \mu_-)\,\mathrm{d}\omega$, shown as dashed curves in Figure 3(a), allows for quantifying the orbital and spin moment using the sum rules [15, 16] according to $m_o = -\frac{4q}{3r} n_h$ and $m_s = -\frac{6p-4q}{r} n_h$, respectively. We omit contributions from the magnetic dipole operator $\langle T_z \rangle$ to the spin moment. While this contribution becomes essential in low-dimensional materials and at interfaces/surfaces due to electron orbital deformation, the alternating atomic monolayers of Fe and Pt atoms cause a substantial normal spin-orbit coupling inherent to $L1_0$ FePt that nullifies asymmetries originating from the surface. Modifications due to slightly different structural and chemical order will not alter these contributions in a significant manner. This is also reflected by the resemblance of literature values. An electron hole density of $n_h = 3.73$ is used for Fe according to first-principle calculations of $L1_0$ FePt [20]. The Fe spin [$m_s = (2.2 \pm 0.2)\ \mu_B$] and orbital [$m_o = (0.24 \pm 0.03)\ \mu_B$] moments per Fe atom are within experimental uncertainty unaffected by the copper concentration [Fig. 3(b)] and agree well with literature values [7, 21–24]. In other words, modifications to magnetic properties, i.e., magneto-crystalline anisotropy, coercive and saturation field, are either not related to the normal Fe magnetic moment and local atomic environment in normal direction, or too small to emerge from the background contributions.

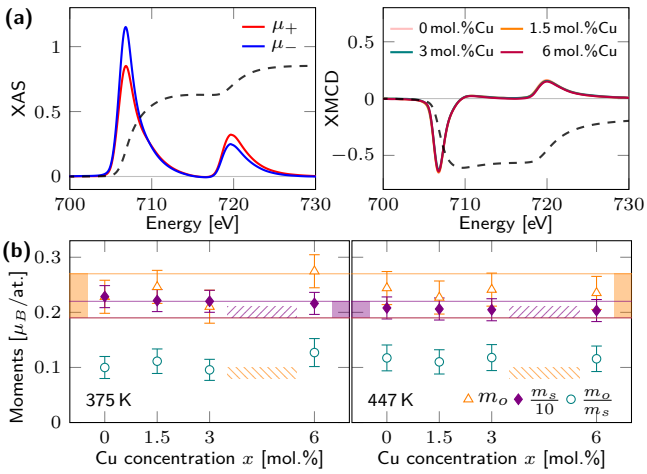

FIG. 3. Spin and orbital moments of Fe quantified by x-ray magnetic circular dichroism spectroscopy. (a) X-ray absorption spectra and XMCD signal near Fe $L_{3,2}$ edges ($2p \rightarrow 3d$) shown for FePt saturated out-of-plane in ± 18.8 kOe. The left panel shows the absorption spectra for 0 mol.%Cu. Dashed lines plot the integrals used for quantitative analysis as defined in the text. (b) Spin and orbital moments as well as their ratio as a function of Cu concentration. Colored horizontal lines indicate literature values for Fe moments in $L1_0$ FePt. Striped lines refer to bcc Fe moments.

Probing the x-ray absorption near the Cu L_3 absorption edge [$(920 \sim 950)$ eV] enables us to directly quan-

tify the Cu electronic configuration, i.e., distribution of the copper coordination environment. We use the same procedure described above for Fe. The Cu XAS spectra exhibit two distinct resonances at 932 eV and 934.2 eV, which are referred to as magnetic Cu and non-magnetic Cu–B, respectively [Fig 4(a)]. This notation is based on ab-initio calculations discussed below. The shaded curves refer to raw data prior to background subtraction of inelastically scattered electrons. The peak height of the second non-magnetic resonance strongly depends on the subtracted background, i.e., Shirley or (inverse tangent) step function. In this respect, we use the average of both background subtractions. The XAS spectra are fitted with two separate product functions consisting of an asymmetric Lorentzian and Gaussian (LG) [Fig 4(b)] [25]:

$$I(E) = h \cdot \mathcal{L}(E - E_0, w, m) \cdot \mathcal{G}(E - E_0, w, 1 - m)\,. \quad (1)$$

Lorentzian and Gaussian are defined as

$$\mathcal{L}(E - E_0, w, m) = \frac{1}{1 + m\left(\frac{E - E_0}{w}\right)^2} \quad (2)$$

and

$$\mathcal{G}(E - E_0, w, m) = \exp\left[-m \log 2 \left(\frac{E - E_0}{w}\right)^2\right], \quad (3)$$

respectively, with the mixing factor m. h and E_0 are peak height and peak location, respectively. The asymmetry of the resonance due to inelastic scattering of excited electrons is described by the energy dependent peak width $w = w_0 + a(E - E_0)$ with the peak asymmetry $a < 10\%$. The shape of the curve is defined by the mixing factor and the peak asymmetry.

For a better comparison, we scale the fits such that the peak height of the low-energy Cu resonance is equal to 1 [lower graph in Fig 4(b)]. Fits for 3 and 6 mol.%Cu samples reveal nearly identical scaled low-energy Cu resonances, and high-energy Cu resonances (Cu–B) that differ only in intensity; both peak position and shape remain constant. Deviations of peak position and shape of the Cu–B resonances of the 1.5 mol.% sample are due to low signal-to-noise ratio causing a fitting uncertainty of $\gtrsim 10\%$. For further analysis, we assume the same transition probability for both resonances. We approximate that the intensity change is directly proportional to the concentration of the Cu atom with the respective electronic configuration. The quantification of the distribution reveals a linear increase of the ratio of Cu-to-Cu–B concentrations and of Cu with total Cu concentration [Fig 4(c)]. In comparison, Cu–B shows only a weak dependence that is overshadowed by a large uncertainty for 1.5 mol.%Cu samples. While low-energy and high-energy Cu L_3 resonances are typically assigned to CuO/Cu(II) and Cu_2O/Cu(I), respectively, the lack of an oxygen atmosphere during deposition and carbon overcoating preventing post-growth oxidation refute this

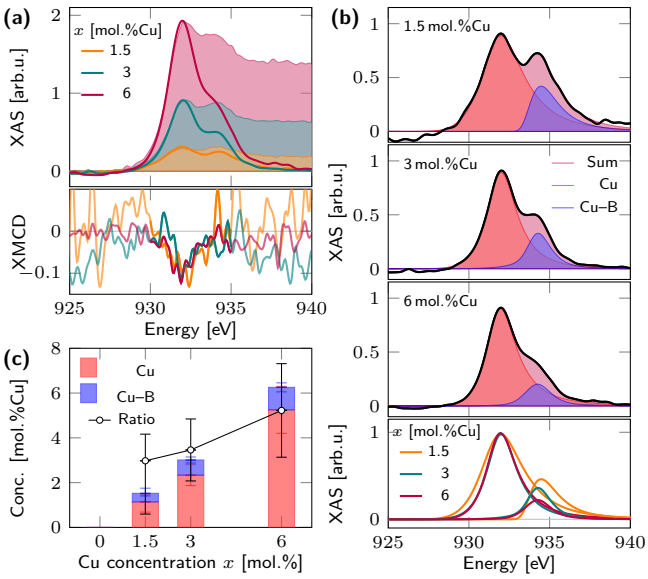

FIG. 4. Copper coordination probed at 375 K with x-ray absorption spectroscopy. (a) Room-temperature XAS and XMCD signal near Cu L_3 edges ($2p \rightarrow 3d$) saturated out-of-plane in ±18.8 kOe. Shaded curves refer to raw data prior to background subtraction of inelastically scattered electrons. (b) Peak fitting using two Lorentzian-Gaussian product functions, as defined in the text, to extract contributions from magnetic Cu and non-magnetic Cu–B resonances. The lower graph plots the fits for all samples. (c) Corresponding absolute and relative Cu concentrations. The black solid curve in (b) refers to the experimental data; the filled curves show the fits with the "sum" resembling the experimental data.

conclusion. The oxidation of copper at grain boundaries is also unlikely as the intercalation of copper into the FePt bulk is energetically preferable. Additionally, the lack of iron oxide signatures makes a claim of copper oxide questionable. In fact, considering an iron-site Cu substitution and a virtually constant interstitial boron concentration explains the occurrence of both Cu and Cu–B resonances, with the latter being nearly unaffected by the total Cu concentration. This aspect is explored in further detail below using ab-initio calculations.

III. AB-INITIO CALCULATIONS

The interpretation of the experimental data is carried out in conjunction with ab-initio calculations of the density of states (DOS) of Cu $3d$ electron orbitals of the energetically most favorable atomic configurations in an $L1_0$ FePt host material. The doping effects on FePt are addressed using a supercell with 32 atoms [Fig. 5(a)], which is sufficiently large to avoid possible interactions of impurities with themselves in periodic systems. We use the generalized gradient approximation [26] as implemented in the Vienna ab-initio simulation package (VASP) [27, 28], and sample the first Brillouin zone

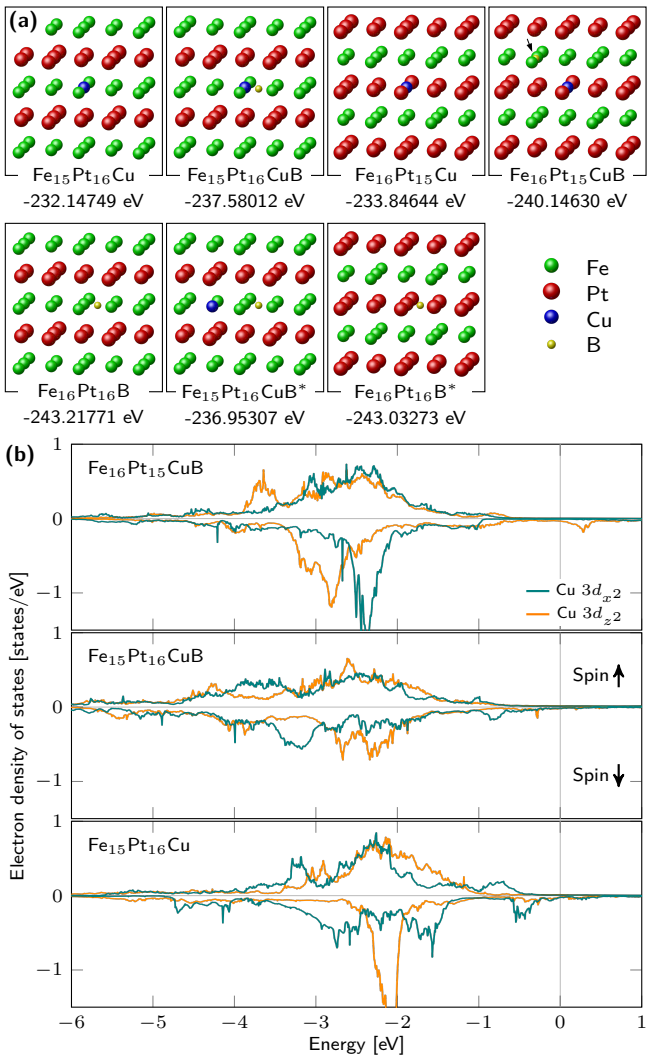

FIG. 5. Ab-initio calculations of $L1_0$ Fe-Pt-Cu-B using VASP. (a) Schematics of 32-atoms supercells displaying energetically most favorable and less favorable (indicated by *) configurations. The corresponding total energies are given below the schematics. Boron is interstitial in the iron sublattice and as close as possible to copper residing either at Fe or Pt sites. (b) Density of states (DOS) of Cu $3d$ electrons near Fermi energy (0 eV) for up and down electron spins plotted on positive and negative axis, respectively. Cu substitution of Pt reveals nearly identical DOS with and without B, and a significant asymmetry along x ($3d_{x^2}$) and z ($3d_{z^2}$). The close proximity of B and Cu on Fe sites causes major changes of the Cu DOS, i.e., degradation of magnetism. Without B, Cu possesses a sizable induced magnetic moment in normal direction. Boron-driven modifications to deeper electron orbitals are minor for given Fe or Pt-site Cu substitution.

with a $9 \times 9 \times 9$ k-point mesh using a kinetic energy cutoff of 520 eV. All considered structures are fully relaxed till the forces between atoms become smaller than 0.1 eV/nm. Afterwards, spin-orbit coupling is activated to determine magnetic moments and total free energy difference for the two cases with out-of-plane and in-plane magnetizations to calculate the saturation magnetization and magnetic anisotropy, respectively. In particular, we start with the $Fe_{16}Pt_{16}$ structure as host material and calculate its magnetic properties. Then, we include Cu atoms as substitutional impurities, replacing either one Fe or one Pt atom, and generate $Fe_{15}Pt_{16}Cu$ and $Fe_{16}Pt_{15}Cu$ structures, respectively. These structures correspond to roughly 3% (1/32) Cu concentration. In contrast, boron doping is modeled as interstitial impurities for $Fe_{16}Pt_{16}B$, $Fe_{15}Pt_{16}CuB$ and $Fe_{16}Pt_{15}CuB$ systems.

Addition of copper or boron reduces the total saturation magnetization and perpendicular magnetic anisotropy, that is attributed to an increased number of delocalized conduction electrons. Boron, which is used to promote nanogranular media in the form of BN segregant in the grain boundary phase, deteriorates the perpendicular magnetic anisotropy when interstitial in the FePt matrix. The specific modifications depend on the composition, location and hybridization of Cu and B atoms [Tab. I]. The relatively small boron atom is interstitial on the Fe sublattice with a 185 meV lower energy compared with boron on the Pt sublattice. For Cu residing at Fe sites, the system gains an energy of 627 meV when Cu and B are in close proximity compared with one lattice constant further away [Fig. 5(a)]. This substantial energy difference ensures Cu–B pairing where possible.

The influence of the atomic configuration on Cu magnetization and band structures is examined in terms of electron density of states (DOS) and shown for the normal (d_{z^2}) and tangential (d_{x^2}) components [Fig. 5(b)]. The experimental data, discussed in the scope of x-ray absorption spectroscopy, refer to $2p_{z^2} \rightarrow 3d_{z^2}$ resonances, which are determined by the electron hole density of states of the $3d_{z^2}$ orbitals, assuming unaffected $2p$ Cu orbitals. The inclusion of Cu into the Fe sublattice of the $L1_0$ host material induces a magnetic Cu moment along the surface normal due to orbital hybridization with Pt, which is drastically altered upon hybridization with boron electron orbitals effectively rendering Cu nonmagnetic. In contrast, the DOS for Pt-site Cu substitution is virtually independent of location and composition of Cu and B atoms due to minimal or absent electron orbital hybridization. Both $Fe_{16}Pt_{15}Cu$ and $Fe_{16}Pt_{15}CuB$ reveal a significant magnetic Cu moment of $(0.12 \sim 0.13)$ μ_B compared with 0.07 μ_B and 0.01 μ_B for $Fe_{15}Pt_{16}Cu$ and $Fe_{15}Pt_{16}CuB$, respectively [Tab. I]. This has to be seen in comparison with elemental nonmagnetic copper. Aside from distinct band asymmetries inducing magnetism, the Cu $3p$ and $3d$ bands are located at slightly different energies. While a direct correlation between numerical and experimental data based on the energy shifts and magnetic moments is not possible due to substantial differences and insufficient signal-to-noise ratio, respectively, the experimental atomic configurations can be identified by the changed magnetic moment with increasing Cu concentration, which is only present in Fe-site Cu substitution. This conclusion, relying on an

TABLE I. Magnetic properties of $L1_0$ Fe-Pt-Cu-B retrieved from ab-initio calculations. Saturation magnetization M_s in kA/m and Bohr magneton per supercell (32 atoms); induced magnetic moment of copper M_s^{Cu} per Cu atom; perpendicular magnetic anisotropy K_u defined as the difference between in-plane and out-of-plane magnetization alignment.

Composition	M_s [kA/m]	M_s [μ_B]	M_s^{Cu} [μ_B]	K_u [MJ/mc]
$Fe_{16}Pt_{16}$	1091	52.698	–	15.85
$Fe_{16}Pt_{16}B$	1050	51.444	–	11.63
$Fe_{15}Pt_{16}Cu$	1038	50.188	0.07	14.14
$Fe_{15}Pt_{16}CuB$	1012	49.865	0.01	8.28
$Fe_{16}Pt_{15}Cu$	1049	52.304	0.13	14.46
$Fe_{16}Pt_{15}CuB$	1049	51.016	0.12	9.89

insufficient amount of interstitial boron to bind with every Cu atom, is corroborated by an enhancement of magnetic properties after N_2 treatment, binding interstitial B as BN in the grain boundary region without altering the Cu location. Additionally, it is in line with lattice parameter modifications suggesting a preferential Fe-site substitution of Cu based on lattice parameters [29]. However, neither results can completely exclude Pt-site Cu substitution due to unchanged background contributions; this probability is significantly smaller, though.

IV. PHENOMENOLOGICAL THEORY OF DISORDERED GRANULAR MEDIA

The competition between degradation of magnetic properties and enhancement of tetragonal crystallographic order in Fe-Pt-Cu-B leads to an optimal Cu concentration in view of maximal perpendicular magnetic anisotropy. Since ab-initio calculations describe bulk materials with perfect ordering at absolute zero temperature, their application to real media is limited owing to finite-size grains, grain size distribution, structural and chemical disorder, and finite temperatures. To overcome these limitations, we propose a phenomenological theory of granular media, parameterized from ab-initio calculations. We extend the phenomenological theory of FePt granular media [5] to include both copper-driven modifications to chemical order of FePt and degradation of its magnetic properties. This approach is based on the overall assumption of a direct relation between perpendicular magnetic anisotropy K_u and coercive field H_c, justified by single-domain switching in individual grains. The modifications to the Curie temperature T_c, saturation magnetization M_s and K_u are treated as perturbations linear in the Cu concentration x. We also assume that the structural order parameter of FePt η depends on x through a phenomenological function $f_\eta(x)$, while its film thickness h and the grain diameter d dependence is the same as in Reference [5]:

$$\eta(d,h,x) = \eta^\infty(h) f_\eta(x) \left[1 - \left(\frac{d_\eta}{d}\right)^{\gamma_\eta}\right], \tag{4}$$

$$f_\eta(x) = 1 - \Delta_\eta \left(1 - \frac{x}{x + x_0}\right)^2. \tag{5}$$

Δ_η, determining the lowest ordering of the $L1_0$ FePt film, is assumed to be 0.5. The critical Cu concentration x_0, governing the shape of $f_\eta(x)$, is set to 5%. We stress that the choice of this value is not based on an experimental reference but chosen in regard to best correlation with experimental data. The structural order parameter $\eta^\infty(h)$ of an extended thin film varies only slightly with film thickness h and is set to $\eta^\infty(3\text{ nm}) \approx 0.8$; d_η is the critical grain diameter below which FePt ordering is lost, and γ_η is the scaling exponent. Generally, Cu doping reduces the exchange energy and lowers the Curie temperature, which is, for perfectly ordered FePt thin films, given by $T_c^{L1_0}(h) - \Delta T_c x$. Similar to Reference [5], we assume a Curie temperature linearly decreasing with the structural order parameter reduction that results in a 150 K lower T_c for completely disordered FePt films compared with perfectly ordered specimens. The diameter dependence of the Curie temperature is universal, and the final expression for T_c becomes:

$$T_c = T_c^\infty \left[1 - \left(\frac{d_0}{d}\right)^{\gamma_{T_c}}\right] \left[T_c^{L1_0}(h) - 150\,\text{K}\left(1 - \frac{\eta(d)}{\eta^\infty}\right) - \Delta T_c x\right], \tag{6}$$

where d_0 and γ_{T_c} are the critical diameter to maintain ferromagnetism and its scaling exponent, respectively. The saturation magnetization of FePt linearly decreases with Cu concentration, which can be accurately quantified with ab-initio calculations as:

$$M_s(d,h,\eta,x,T_c,T=0) = M_s(d,h,\eta,T_c,T=0) - \Delta M_s x\,. \tag{7}$$

The temperature dependence of magnetization is given by the function f_m [5]:

$$f_m(d,h,\eta,x,T_c) = \frac{M_s(d,h,\eta,x,T_c)}{M_s(d,h,\eta,x,T_c,T=0)} = \left[1 - s\left(\frac{T}{T_c(d,h,\eta,x)}\right)^{3/2} - (1-s)\left(\frac{T}{T_c(d,h,\eta,x)}\right)^p\right]^{1/3}. \tag{8}$$

The magnetic anisotropy of perfectly ordered FePt films at $T = 0$ K linearly decreases with Cu in the low concentration limit. This Cu doping effect is given by $K_u^{L1_0}(h, T=0) - \Delta K_u x$, which is quantified by ab-initio calculations.

Accounting for the grain diameter, structural order parameter and temperature dependence results in the following expression:

$$K_u(d,h,\eta,x,T_c) = \left(K_u^{L1_0}(h,T=0) - \Delta K_u x\right)\left[1-\left(\frac{d_{K_u}}{d}\right)^{\gamma_{K_u}}\right]\left(\frac{\eta(d,h,x)}{\eta^{\infty}(h)}\right)^2 f_{K_u}(d,h,\eta,x,T_c,T)\,, \tag{9}$$

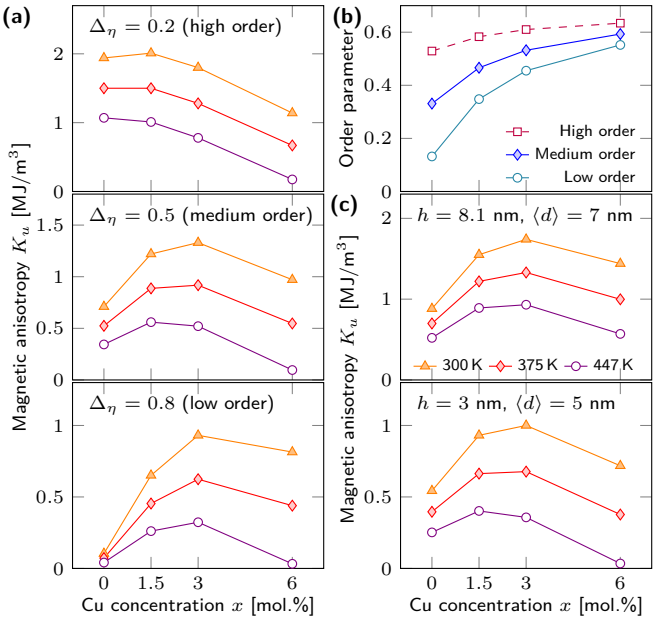

FIG. 6. Phenomenological description of copper concentration dependence of magnetic properties. (a) Perpendicular magnetic anisotropy K_u for high, medium and low initial ordering of $L1_0$ FePt at different temperatures. Calculations are performed for cylindrical granular media with diameter (7 ± 1.8) nm, film thickness 3 nm, Curie temperature $T_c^{L1_0}(7\text{ nm}) = 650$ K, and a 0.2 nm-thick dead layer. (b) Corresponding structural order parameters improving with Cu concentration. (c) Perpendicular magnetic anisotropy K_u for films with different grain volume and $\Delta_\eta = 0.5$ revealing same effect of Cu addition with a different magnitude.

where d_{K_u}, γ_{K_u} and f_{K_u} are the critical diameter, critical exponent and a function describing temperature dependence of magnetic anisotropy, respectively. The averaged magnetic properties of granular media are obtained from corresponding magnetic properties of a single grain with diameter d assuming a Gaussian distribution of the grain diameters with an mean diameter $\langle d\rangle$ and a standard deviation σ_d. Note that the film thickness does not explicitly enter the model.

The calculations are performed for media with two different film thicknesses, i.e., $h = 8.1$ nm and $h = 3$ nm, consisting of cylindrical grains with $\langle d\rangle = 8.1, 7, 5, 3$ nm, $\sigma_d = 1.8$ nm, $T_c^{L1_0}(8.1\text{ nm}) = 720$ K, $\eta^{\infty}(8.1\text{ nm}) = 0.85$, and $K_u^{L1_0}(8.1\text{ nm}, 0\text{ K}) = 7.7$ MJ/m^3; and $\langle d\rangle = 8.1, 7, 5, 3$ nm, $\sigma_d = 1.8$ nm, $T_c^{L1_0}(3\text{ nm}) = 650$ K, $\eta^{\infty}(3\text{ nm}) = 0.8$, and $K_u^{L1_0}(3\text{ nm}, 0\text{ K}) = 6.9$ MJ/m^3.

We consider three cases for which the initial Cu-free ordering of FePt is relatively good, medium and poor [Fig. 6(a)]. For either case, the structural order parameter of FePt described by $f_\eta(x)$ increases with the Cu concentration [Fig. 6(b)]. While high-quality $L1_0$ FePt films show a steady decline of the perpendicular magnetic anisotropy with increasing Cu concentration, systems with a low initial quality exhibit a non-monotonic behavior [Fig. 6(a)] similar to the experimentally observed coercivity [Fig. 2(b)]. This is because of the competition between copper-driven structural order parameter improvement and degradation of magnetic properties, such as Curie temperature, saturation magnetization and magneto-crystalline anisotropy. For initially high-quality films ($\eta \gtrsim 0.8$), the structural order parameter improvement with Cu concentration is marginal and degradation of magnetic properties is a dominant effect, consistent with our ab-initio calculations. Lower-quality films experience a strong effect of structural order parameter improvement that substantially increases K_u up to a Cu concentration of 3%. At this pivotal point, the degradation of magnetic properties takes over leading to a non-monotonous K_u vs. x dependence. From a practical point of view, the change of magnetic properties can be used to judge original and current film qualities. Calculations for different grain volumes shows the same qualitative trend of the Cu concentration dependence of magnetic properties because intrinsic magnetic properties are determined from experiment and ab-initio calculations, and extrinsic properties, stemming from varying grain volumes, solely affect the magnitude of the effect [Fig. 6(c)].

V. CONCLUSION

We investigated the effect of boron and copper additions ($\lesssim 6$ mol.%Cu) on structural and magnetic properties of $L1_0$ FePt granular media. The formation of nanogranular media was governed by boron virtually independent of the Cu concentration. Coercive/saturation field and perpendicular magnetic anisotropy increased with Cu concentration up to 3 mol.%Cu owing to a promoted tetragonal crystallographic order of $L1_0$ FePt. Samples with larger copper concentration suffered from an intrinsic degradation of magnetic properties in Fe-Pt-Cu-B films, associated with delocalized electron orbitals originating from a larger d-orbital occupancy in Cu than in Fe. Generally, total magnetic moment, magnetic anisotropy and Curie temperature were reduced by

either B or Cu addition. The interplay between enhancement of crystallographic order and degradation of magnetic properties was analytically treated by advancing the phenomenological theory of FePt granular media to include copper-driven modifications. We quantified both spin and orbital moments of iron along the surface normal, and determined the electronic configuration of Cu. No modifications to the Fe configuration were observed. The ratio of magnetic Cu to non-magnetic Cu–B concentration increased linear with the total Cu concentration, indicating a Cu population of the Fe sublattice and a nearly constant concentration of interstitial boron. The preferred atomic configurations were obtained from ab-initio calculations and analyzing the density of states of Cu 3*d* electron orbitals. Our results showcase the importance of joint experimental and theoretical studies to advance synthesis capabilities particularly in view of magnetic hard-drives.

ACKNOWLEDGMENTS

This work was funded by the U.S. Department of Energy, Office of Science, Office of Basic Energy Sciences, Materials Sciences and Engineering Division under Contract No. DE-AC02-05-CH11231 (NEMM program MSMAG). This research used resources of the Advanced Light Source, which is a DOE Office of Science User Facility under contract no. DE-AC02-05-CH11231.

[1] D. Weller, G. Parker, O. Mosendz, E. Champion, B. Stipe, X. Wang, T. Klemmer, G. Ju, and A. Ajan, A HAMR Media Technology Roadmap to an Areal Density of 4 Tb/in^2, IEEE Trans. Magn. **50**, 1 (2014).

[2] D. Weller, O. Mosendz, G. Parker, S. Pisana, and T. S. Santos, L10 feptx–y media for heat-assisted magnetic recording, Phys. Status Solidi A **210**, 1245 (2013).

[3] D. Weller, G. Parker, O. Mosendz, A. Lyberatos, D. Mitin, N. Y. Safonova, and M. Albrecht, Review article: Fept heat assisted magnetic recording media, J. Vac. Sci. Technol. B **34**, 060801 (2016).

[4] A. Perumal, Y. Takahashi, T. Seki, and K. Hono, Particulate structure of l10 ordered ultrathin fept films for perpendicular recording, Appl. Phys. Lett. **92**, 132508 (2008).

[5] Y. Zhang, A. Kalitsov, J. Ciston, O. Mryasov, B. Ozdol, J. Zhu, S. Jain, B. Zhang, B. Livshitz, A. Chernyshov, A. Ajan, P. Dorsey, G. Bertero, R. Acharya, A. Greene, and S. Myers, Microstructure and magnetic properties of ultrathin fept granular films, AIP Adv. **8**, 125018 (2018).

[6] H. Sepehri-Amin, M. Nagano, T. Seki, H. Ho, D. Tripathy, S. Pirzada, K. Srinivasan, H. Yuan, P. Dorsey, A. Ajan, and K. Hono, Microstructure and magnetic properties of fept-(c,sio2) granular films deposited on mgo, mgtio, and mgtion underlayers, Scripta Materialia **157**, 1 (2018).

[7] R. Streubel, A. T. N'Diaye, K. Srinivasan, A. Ajan, and P. Fischer, Origin of enhanced anisotropy in fept-c granular films revealed by xmcd, Appl. Phys. Lett. **114**, 162401 (2019).

[8] C. Platt, K. Wierman, E. Svedberg, R. van de Veerdonk, J. Howard, and D. Roy, A.G.and Laughlin, L–10 ordering and microstructure of fept thin films with cu, ag, and au additive, J. Appl. Phys. **92**, 6104 (2002).

[9] K. Wang, B.and Barmak, Re-evaluation of the impact of ternary additions of ni and cu on the a1 to l10 transformation in fept films, J. Appl. Phys. **109**, 123916 (2011).

[10] R. K. Dumas, Y. Fang, B. J. Kirby, C. Zha, V. Bonanni, J. Nogués, and J. Åkerman, Probing vertically graded anisotropy in feptcu films, Phys. Rev. B **84**, 054434 (2011).

[11] D. A. Gilbert, L.-W. Wang, T. J. Klemmer, J.-U. Thiele, C.-H. Lai, and K. Liu, Tuning magnetic anisotropy in (001) oriented $L10(Fe_{1x}Cu_x)_{55}Pt_{45}$ films, Appl. Phys. Lett. **102**, 132406 (2013).

[12] S. Jain, C. Papusoi, R. Admana, H. Yuan, and R. Acharya, Magnetization reversal process and evaluation of thermal stability factor in cu doped granular l10 fept films, J. Appl. Phys. **123**, 193902 (2018).

[13] K. Sharma, G. Sharma, M. Gupta, V. R. Reddy, and A. Gupta, Enhancement of l10 transformation in fe/pt multilayer by cu addition, AIP Advances **8**, 105118 (2018).

[14] J.-C. Chiu, W.-C. Wen, L.-W. Wang, D.-S. Wang, and C.-H. Lai, Effects of b additions in fept and fept:c films, J. Appl. Phys. **115**, 17B713 (2014).

[15] B. T. Thole, P. Carra, F. Sette, and G. van der Laan, X-ray circular dichroism as a probe of orbital magnetization, Phys. Rev. Lett. **68**, 1943 (1992).

[16] P. Carra, B. T. Thole, M. Altarelli, and X. Wang, X-ray circular dichroism and local magnetic fields, Phys. Rev. Lett. **70**, 694 (1993).

[17] D. A. Shirley, High-resolution x-ray photoemission spectrum of the valence bands of gold, Phys. Rev. B **5**, 4709 (1972).

[18] C. T. Chen, Y. U. Idzerda, H.-J. Lin, N. V. Smith, G. Meigs, E. Chaban, G. H. Ho, E. Pellegrin, and F. Sette, Experimental confirmation of the x-ray magnetic circular dichroism sum rules for iron and cobalt, Phys. Rev. Lett. **75**, 152 (1995).

[19] K. Ikeda, T. Seki, G. Shibata, T. Kadono, K. Ishigami, Y. Takahashi, M. Horio, S. Sakamoto, Y. Nonaka, M. Sakamaki, K. Amemiya, N. Kawamura, M. Suzuki, K. Takanashi, and A. Fujimori, Magnetic anisotropy of l10-ordered fept thin films studied by fe and pt l2,3-edges x-ray magnetic circular dichroism, Appl. Phys. Lett. **111**, 142402 (2017).

[20] S. Miwa, M. Suzuki, M. Tsujikawa, K. Matsuda, T. Nozaki, K. Tanaka, T. Tsukahara, K. Nawaoka, M. Goto, Y. Kotani, T. Ohkubo, F. Bonell, E. Tamura, K. Hono, T. Nakamura, M. Shirai, S. Yuasa, and Y. Suzuki, Voltage controlled interfacial magnetism through platinum orbits, Nat. Commun. **8**, 15848 (2017).

[21] O. Dmitrieva, M. Spasova, C. Antoniak, M. Acet, G. Dumpich, J. Kästner, M. Farle, K. Fauth, U. Wiedwald, H.-G. Boyen, and P. Ziemann, Magnetic moment

of fe in oxide-free fept nanoparticles, Phys. Rev. B **76**, 064414 (2007).

[22] D. Xu, C. Sun, J. Chen, S. Heald, B. Sanyal, R. Rosenberg, T. Zhou, and G. Chow, Large enhancement of magnetic moment in $l1_0$ ordered FePt thin films by nd substitutional doping, J. Phys. D: Appl. Phys. **48**, 255001 (2015).

[23] S. Sakamoto, K. Srinivasan, R. Zhang, O. Krupin, K. Ikeda, G. Shibata, Y. Nonaka, Z. Chi, M. Sakamaki, K. Amemiya, A. Fujimori, and A. Ajan, Effects of cobalt substitution in $l1_0$ -(fe,co)pt thin films, Phys. Rev. B **96**, 144437 (2017).

[24] J. Wang, H. Sepehri-Amin, H. Tajiri, T. Nakamura, K. Masuda, Y. Takahashi, T. Ina, T. Uruga, I. Suzuki, Y. Miura, and K. Hono, Impact of carbon segregant on microstructure and magnetic properties of FePt-C nanogranular films on MgO (001) substrate, Acta Mater. **166**, 413 (2019).

[25] R. Ansell, T. Dickinson, A. Povey, and P. Sherwood, X-ray photoelectron spectroscopic studies of electrode surfaces using a new controlled transfer technique: Part ii. results for a molybdenum electrode and the curve fitting procedure, J. Electroanal. Chem. **98**, 79 (1979).

[26] J. P. Perdew, K. Burke, and M. Ernzerhof, Generalized gradient approximation made simple, Phys. Rev. Lett. **77**, 3865 (1996).

[27] G. Kresse and J. Hafner, Ab initio molecular dynamics for liquid metals, Phys. Rev. B **47**, 558 (1993).

[28] G. Kresse and J. Furthmüller, Efficiency of ab-initio total energy calculations for metals and semiconductors using a plane-wave basis set, Comput. Mater. Sci. **6**, 15 (1996).

[29] Y. Takahashi, M. Ohnuma, and K. Hono, Effect of cu on the structure and magnetic properties of fept sputtered film, J. Magn. Magn. Mater. **246**, 259 (2002).